Why is cancer not more common? A changing microenvironment may help to explain why, and suggests strategies for anti-cancer therapy

Xiaowei Jiang* and Ian P.M. Tomlinson*

Cancer Genetics and Evolution Laboratory, Institute of Cancer and Genomic Sciences, College of Medical and Dental Sciences, Vincent Drive, University of Birmingham, Edgbaston, Birmingham B15 2TT, United Kingdom

*Corresponding authors: Xiaowei Jiang (x.jiang.4@bham.ac.uk), Ian P.M. Tomlinson (i.tomlinson@bham.ac.uk)

Abstract

One of the great unsolved puzzles in cancer biology is not why cancers occur, but rather, explaining why so few cancers occur compared with the theoretical number that could occur given the number of progenitor cells in the body and the normal mutation rate. We hypothesised that a contributory explanation is that the tumour microenvironment (TME) is not fixed, and that this could impair the ability of neoplastic cells to retain a high enough fitness to become a cancer. The TME has implicitly been assumed to be static in most cancer evolution models, and we therefore developed a mathematical model of spatial cancer evolution assuming that the TME, and thus the optimum cancer phenotype, change over time. Based on simulations, we show how cancer cell populations adapt to diverse changing TME conditions and fitness landscapes. Compared with static TMEs which generate neutral dynamics, changing TMEs lead to complex adaptations with spatio-temporal heterogeneity involving variable sub-clonal fitness, mixing, competition and phylogeny patterns. In many cases, cancer cell populations fail to grow or undergo spontaneous regression, and even extinction. Our analyses predict that cancer evolution in a changing TME is challenging, and can help to explain why cancer is neither inevitable nor as common as expected. Should cancer driver mutations with effects dependent of the TME exist, they are likely to be selected. Anti-cancer prevention and treatment strategies based on changing the TME are feasible and potentially effective.

Introduction

Although cancer is viewed as a common disease, our current knowledge of how cancers grow suggests that cancer is actually far less frequent than we expect[1]: the mutation rates and number of normal cells suggest that many cancers could occur in each human. There are several potential reasons for the "cancer deficiency", including anti-cancer immune responses[2] and inherent mechanisms of tissue homoeostasis (or "buffering")[3]. We hypothesised that a further contributory factor restraining carcinogenesis is that the tumour microenvironment (TME) is not fixed, and that this could impair the ability of neoplastic cells to retain a high enough Darwinian fitness to become a cancer.

Carcinogenesis has long been viewed as an ecological and evolutionary process[4-10], epitomized by Nowell's illustrated phylogenetic model in which clonal and stepwise accumulation of advantageous mutations under selection from the tumour microenvironment (TME) cause a cancer to grow[5]. Although the seminal ideas proposed by Nowell and others[5,11] – have guided cancer research for decades, a general theory of adaptive cancer evolution is lacking[6,8-10,12]. Some fundamental questions remain unanswered, including the role of a changing TME in determining the fitness of mutations and the evolutionary trajectories of cancers in three-dimensional (3D) tissue space. Does cancer evolution proceed by driver mutations with large effects, small effects or a combination of both? How and why does the fitness of driver mutations differ across cancer types? What spatio-temporal patterns of cancer development can be observed under different tempos and modes of adaptive evolution?

Factors intrinsic to the cancer cell, such as mutations and stable epigenetic features, and the TME should jointly determine the tumour's evolutionary trajectory [1,5,13-18]. The TME can include many non-neoplastic cells and acellular components, including stromal constituents such as fibroblasts, immune cells, the extracellular matrix (ECM) and the pre-metastatic niche. These features may, in part, be caused by the cancer cell itself. The TME is thought to be a dynamic influence on tumour progression and metastasis [1,15,19-23], and spatially varying immune TME[2] and cycling hypoxic TME play important roles in driving cancer evolution [24,25]. Conceptually, cancer development can be viewed as an

adaptive evolution process in a changing microenvironment, where the cancer cell survives if its phenotype is close to the optimum resulting from cell-intrinsic (cell-autonomous) factors and the TME.

In previous ecological and evolutionary modelling of cancer, different aspects of cancer development and treatment , such as tumour initiation and progression, cell-cell interactions and TME effects, have been studied using a plethora of ecological, evolutionary and mathematical approaches (for example, [26,27]). However, due to challenges in modelling the TME explicitly, the fitness effect of mutations has usually been pre-specified and the TME has been rather neglected [28,29]. When the TME has specifically been considered as a source of selection [13,30,31], the underlying genetic basis – such as the variable fitness effects of driver mutations – has not been explicitly considered. Moreover, the important question of how cancer cells adapt in a TME with a changing phenotypic optimum, for example due to a variable immune response[18], has not generally been considered.

To address these issues within the same evolutionary and ecological framework, with the dual aims of providing a general model of adaptive cancer evolution and investigating the effects of a changing TME on cancer growth, we set up a mathematical model of carcinogenesis as an adaptive evolutionary process. In this model, the cancer cells and their changing phenotypic optimum caused by the TME jointly determine the cancer's evolutionary trajectory. The results of the simulations help to explain why cancer growth is unpredictable, unstable and uncertain process, with implications for anti-cancer strategies.

Results

Description of the model

Our model, which is based on Fisher's classical phenotypic geometric model[12,32], considers a tumour that comprises multiple neoplastic cells, each of which has a phenotype determined by random mutations and a Darwinian fitness determined by how far the phenotype is from an optimum determined in part by the TME. The adaptive

process Fisher described is analogous to adjusting the knobs of a microscope (mutations) and each resulting trait contributes to fitness independently (universal pleiotropy)[33]. In Fisher's original analogy, the object on the microscope's stage is static, so the population adapts to a static phenotypic optimum in that environment. In our model, we assume that the TME has a phenotypic optimum that follows various changing patterns. In each cancer cell, the changing phenotypic optimum leads to continual selection acting on the fitness effect of mutations that influence the phenotypic traits of cancer cells.

To model the above adaptive process, our model uses fitness landscapes (Supplementary Figures S1 and S2), with a single changing phenotypic optimum determined by the TME (see Methods for model details and Supplementary Figure S1). The model can also consider cell-autonomous mutations which we assume to act independently of the TME. In a very simple landscape, the fitness of a cancer cell with two traits can be described by a function in a three-dimensional Cartesian co-ordinate system, where the height along the fitness surface corresponds to fitness and the other two co-ordinates correspond to phenotypic values of each trait. The initial optimal phenotypic value defining the maximum fitness is at the origin of the Cartesian coordinate system, which points to the initial "peak" of the fitness landscape (Supplementary Figure S2). The optimum can move, directionally or otherwise (e.g. randomly or cyclically, see Methods), as the phenotypic optimum changes.

Mutation rate and the number of loci are specified before each simulation. The former could, for example, be increased owing to aberrations in key pathways maintaining DNA replication fidelity, or extrinsic mutagens (Supplementary Figure S1b). A computer simulation of cancer evolution then proceeds in the following fashion (Supplementary Figure S1a). At each generation, the initial fitness ($w_0 = w(\mathbf{z}_0)$) of each cancer cell is conferred by a starting phenotype, $\mathbf{z}_0$, which is unchanged from the previous generation unless a new mutation (advantageous or deleterious) occurs by chance, or phenotypic plasticity arises, for example from disturbances such as inflammation [15]. The phenotypic effect (size) of a mutation is sampled from a multivariate normal distribution. A

mutation with large fitness effect can move the cancer cell a long phenotypic distance relative to its phenotypic optimum in the fitness landscape. The changing phenotypic optimum of the TME can also change each cancer cell's fitness. When the cell phenotype and/or phenotypic optimum changes, the Euclidean distance, d, of the phenotype from the optimum will change to d', with an associated higher or lower fitness value $w(d')$. All these changes in fitness naturally lead to different levels of selection and adaptation – a cancer cell acquires higher fitness when mutations move its phenotype closer to the optimum. Depending on the fitness effects of the mutations in that cell and position of the phenotypic optimum at generation, *t*, we assume that every cancer cell has to survive viability selection according to its birth rate (the probability to give daughter cells during viability selection – equivalent to its fitness at generation *t*), $w(\mathbf{z},t)$ and death rate (the probability of cell death during viability selection), $1-w(\mathbf{z},t)$.

The surviving cancer cells then reproduce asexually. New daughter cells randomly occupy available tissue space in 3D according to pre-specified limits on tumour size that may vary with time. The tumour may go extinct, persist with varying size, or grow continuously until it reaches its maximum allowed space or size (nominally representing clinical presentation), after which it continues to be under viability selection without expanding. If an allele becomes fixed in the population, we say this is an adaptive or positively selected driver mutation, even if subsequent phenotypic optimum changes render that driver mutation disadvantageous or neutral. This does not exclude the possibility that mutations may apparently be "selected" due to hitch hiking, even including variants with negative fitness coupled to a mutation with a stronger, positive effect. Competition between tumour sub-clones (or "clonal interference") can occur as a consequence of limits we optionally set on tumour size.

Cancer adaptation under diverse cancer initiation conditions and a changing phenotypic optimum

In our modelling framework, we make some general, plausible assumptions for cancer initiation and phenotypic optimum change dynamics, such that the neoplastic growth

can be initiated by a single stem cell with any initial fitness. In some cases, we assume that the cell population has undergone a modest initial expansion analogous to a benign cancer precursor lesion [34]. We simulate cancer evolution under various initial fitness conditions and phenotypic optima.

First, we simulate cancer evolution with a static phenotypic optimum ($v_1 = 0$, see Methods). A single cell with two traits ($n = 2$) starts asexual reproduction from the centre of a 3D tumour tissue space with a phenotype at the optimum with initial fitness $w_0 = 1$. This assumption is used to simulate a stem cell with an optimum fitness conferred by a driver mutation, which is ensured to form a cancer with initial cell-autonomous phenotype and growth in its local TME. The cancer starts to grow with cell birth rate, $w(\mathbf{z},t)$, and death rate, $1 - w(\mathbf{z},t)$. The cancer undergoes classical constant stabilising selection, where purifying selection removes cells with deleterious mutations. The mean cancer population fitness remains high and does not fluctuate in time or space (Supplementary Movie S1). When under constant stabilising selection, we find that there is no fixation of any new driver mutations (Supplementary Figure S3 and Movies S1), consistent with the "big bang" model of tumorigenesis in colorectal cancer[29].

Once any type of changing TME – and hence changing phenotypic optimum – is imposed, several interesting patterns of evolution emerge. The fluctuating fitness of cancer cells in time and space caused by a moving phenotypic optimum and random mutations can result in complex patterns of clonal and sub-clonal evolution (Supplementary Movies S2-S6). Different morphologies based on varying clonal or sub-clonal population structures can emerge (see examples in Figure 1). The speed of phenotypic optimum change is critical. If the phenotypic optimum moves too fast, and the cancer cells do not acquire enough beneficial mutations to increase mean population fitness, the population goes extinct (Supplementary Movies S2-S4). However, if the optimum moves at a moderate speed the cancer population may acquire enough beneficial mutations to "catch up" with the phenotypic optimum (Supplementary Movies S5-S6). If the optimum moves slowly, the tumour can grow almost exponentially to the maximum space and/or

population size allowed ($N = 10^7$), typically forming a ball (Supplementary Movies S5-S6), and then continue to evolve with few new driver mutations.

We find two general clonal or sub-clonal growth patterns in 3D: (i) one or more balls of cells (Figure 1a-i); or (ii) irregular morphology (Figure 1j-l). Intriguingly, these patterns generally resemble those observed clinically [20,28]. As a fast-changing TME often leads to fast cell turnover, we are more likely to observe ball-like structures (Figure 1a-l, Supplementary Movies S3-S6). Moreover, fast-changing TMEs can lead to many smaller sub-clones, which turn over fast, with fluctuating numbers, spatial proximity and fitness (Figure 1a-c, Supplementary Movies S3). We also find that sub-clonal populations mix frequently with variable fitness and spatio-temporal heterogeneity during evolution (Figure 1, Supplementary Movies S2-S6). In a relatively static or an extremely slow-changing TME, spatio-temporal clonal turnover is slow and the cancers shows an irregular morphology more frequently (e.g., see Figure 1g-l, Supplementary Movies S6). This is because selection is quite weak and hence adaptive evolution is limited. Moreover, to understand the fitness effects of selected driver mutations in a changing TME, we measured the mean population fitness and the mean fitness advantage of selected driver mutations, which are mostly determined by the speed of phenotypic optimum change (Figure 2, Supplementary Movies S2-S6). As expected, the mean population fitness decreases faster in a fast-changing TME, whereas a slow-changing/static TME leads to slower fitness decay and thus longer survival time of the tumour. Lower selection intensities (a "flatter" fitness landscape; Supplementary Figure S2) can also mitigate against a changing TME, significantly increasing mean fitness of the cancer cell population (Supplementary Figures S4-S6).

Second, we now consider that the population starts from a phenotype away from the optimum, and thus has lower initial fitness ($w_0 < 1$). If the initial fitness is relatively low (e.g., $w_0 = 0.1$), the chance of population extinction is high (Figure 3, Supplementary Movies S7-S11). We conclude that in this scenario, a cancer is much more likely to grow if it is initiated by a cell-autonomous driver mutation conferring relatively high fitness that has small or zero dependency on the TME. This means that relatively low fitness

cells can gain higher fitness and, with a larger "initial" population size, have a higher chance of generating appropriate driver mutations to survive selection due to either sudden or rapid phenotypic optimum change. If the population survives the initial selection, and assuming that the phenotypic effects of subsequent mutations are TME-dependent, its evolutionary trajectory will depend on the rate of phenotypic optimum change (Figure 3, Supplementary Movies S8-S15). Again, our simulations show three similar patterns as above. First, a fast-changing TME leads to selection of driver mutations with large fitness advantage and quick population extinction, which, however, can be delayed if the initial population size is large (Figure 3d, h and l). Second, a moderately fast-changing TME promotes cancer adaptation by fixing more driver mutations (Figure 3b, f and j, Supplementary Movies S9, S13). Third, if the population evolves under a slowly changing TME, we recover subsequent driver mutations that have small fitness effects (Figure 3a, e and i, Supplementary Movies S7, S15). These mutations could be termed "mini-drivers", as we proposed previously[35]. These results show that cancer is unlikely to reach an optimum by using major drivers alone. Further exploration of three mechanisms potentially affecting cancer adaptation – chromosome instability, selection correlation and cell-TME interaction – is shown in Supplementary Figures S7-S10 and Supplementary Notes 1-3.

Next, to understand how other types of changing phenotypic optimum affect cancer adaptation, we analyse another three types of changing TME (randomly fluctuating, directionally changing with a randomly fluctuating component and cyclic). These results show similar patterns to the directionally changing optimum, indicating that our conclusions regarding highly uncertain evolutionary trajectories caused by changing TME are robust. There are, however, some novel patterns observed when the TME changes in a non-directional fashion, such as that a cycling phenotypic optimum is particularly capable of promoting adaptive evolution by periodically fixing more driver mutations (Supplementary Figures S11-S13, Supplementary Movies S16-S17, Supplementary Note 4). In general, a directionally changing optimum more likely causes reduced mean population fitness and thus more killing of cancer cells. Moreover, addition of random fluctuation in the phenotypic optimum can lead to further killing of cancer cells.

Finally, we explore how various changing TMEs and phenotypic optima change dynamics shown above affect sub-clonal cell-cell competition and properties of driver mutations, especially their genotypic landscapes (see Methods). We show that changing TMEs can generate genotypic landscapes of considerable ruggedness and sign epistasis, meaning that predicting cancer adaptation from the complement of driver mutations may be misleading in this scenario. Further explorations of sub-clonal cancer evolutionary dynamics under a changing TME are shown in Supplementary Figures S14-S24, Supplementary Movies S18-S21 and Supplementary Notes 5-6.

Both changing a phenotypic optimum and spatial constraints on population size affect cancer phylodynamics and adaptation

To understand the effects on cancer phylodynamics of variable selection caused by a changing TME (see Methods), we reconstruct cancer phylogenies in the simulations shown above within a 3D TME space of the same size. Intriguingly, we find that in all cases the shapes and the temporal signals in the phylogenies (e.g., the local branch length and overall shape) are characteristic of the particular optimum change dynamics, that is, TMEs with the phenotypic optimum changing at different speeds (illustrated in Figure 4). In all cases phylogenies from a slowly changing TME, have long parallel branches indicating that sub-clones may co-exist for long periods of time without fixation (Figure 4**a-b**), indicating weak selection on sub-clones. A moderately fast-changing optimum (Figure 4**c**) typically leads to continual selection of branches with beneficial mutations and thus favours adaptive evolution. A fast-changing phenotypic optimum causes strong selection and shorter branches indicating fast extinction of the sub-clones (Figure 4**d**). Similar results are obtained for other optimum change dynamics (illustrated in Supplementary Figure S25).

As the available cancer niche space may also affect cancer adaptation and phylodynamics, for example eliminating less fit cancer cells, we repeat the simulations shown above using the three (directional, cyclic and random) phenotypic optimum change dynamics with different spatial constraints on cancer size and reconstructed all

phylogenies during the simulations. We further use two measures for quantifying asymmetry of these phylogenies, the normalised Sackin's index and the number of cherries (see Methods), respectively. We find that both spatial constraints and a changing phenotypic optimum can affect cancer adaptation and phylodynamics to various degrees (Supplementary Figure S26-S27, Supplementary Note 7). Particularly, when the changing TME causes strong selective pressure smaller 3D space hinders adaptive evolution while larger 3D space promotes it.

Cancer adaptation owing to anti-cancer therapies

Given our finding that a changing TME tends to promote cancer extinction or sub-optimal growth, we now extend our model to simulate the effects of different anti-cancer therapeutic strategies, by assuming that these modify the phenotypic optimum and/or the shape of the fitness landscape (see equation (17), Supplementary Figure S2). We examine the effects of treatments such as genotoxic therapies (radiotherapy or chemotherapy)[36] and immunotherapy [2] by assuming they can cause a sudden shift in the phenotypic optimum and hence place cancer cells under strong selective pressure. For simplicity, we assume that the therapy causes the optimum to move suddenly to various degrees along the axis of the first trait while keeping the optimum constant at the rest (Supplementary Figure S28), our intention being to determine qualitatively what happens with a treatment-induced phenotypic optimum shift. We confirm that although all treatments assumed to be effective are successful in reducing mean population fitness and tumour mass to the brink of extinction ($w \leq 0.1$), only treatments that induce the very large optimum shifts can cause cure (Supplementary Figure S28, Supplementary Movies S22-S25). Moreover, the complementary phylogenies also show that the selection from the treatment induced optimum shifts often leads to expansion of sub-clones and extinction of the majority of the tumour mass (Supplementary Figure S29). Weak treatment leads to a large number of initial sub-clones with *de novo* resistance mutations, but eventually the tumour mass comes to be dominated by a single sub-clone (Supplementary Figure S29) carrying the mutation with the largest selective advantage. Stronger, but non-lethal, treatment leads to an early sub-clonal expansion

carrying the mutation with a very large selective advantage ($s = 26.563$, Supplementary Figure S28).

In terms of sub-clonal diversity, we observe a reduction soon after treatment and then an increase, but after sub-clonal fitness recovers to the same or similar levels as those at pre-treatment, diversity reduces again until the end of the treatment (data not shown). These behaviours are consistent with a mean population fitness decrease due to treatment and selection for resistant sub-clones (Supplementary Figure S29). Interestingly, our simulations show that most resistance mutations are born early but not pre-existing. In rare cases, the few pre-existing resistance mutations are deleterious, suggesting they moved these mutant sub-clones' phenotypes away from the original optimum and the treatments actually helped those sub-clones to survive by moving their phenotype closer to the new treatment-induced optimum. Moreover, when the treatments lead to a sufficiently high selection intensity (a "narrower" fitness peak, see Supplementary Figure S2), all treatments lead to immediate cure (population extinction).

To understand potential therapeutic resistance, we examine three mechanisms that cancers could use to increase mean population fitness and avoid extinction (Supplementary Movies S26-S28, Supplementary Figure S30). First, we assume a polygenic model of resistance, which has quantitative traits. Somatic copy number variation may increase the number of genetic loci contributing to resistance, which helps the population avoid extinction and select for resistance driver mutation ($L = 50$, Supplementary Figure S30a). Second, with an elevated mutation rate – perhaps caused by the therapy itself –mean population fitness can quickly rebound and avoid extinction, where positively selected resistance mutations arise during the simulation (Supplementary Figure S30b). Interestingly, all positively selected resistance mutations found have a *de novo* origin after treatment initiation, because all other mutations in sub-clones are removed by therapeutic selection or failed to hitchhike within the dominant sub-clone. Third, if the selection intensity decreases, for example therapy intensity is reduced owing to toxicity, the cancer population can also avoid extinction (

$\sigma^2 = 40$, Supplementary Figure S30c, the fitness landscape shape change is illustrated in Supplementary Figure S30). Nevertheless, due to weaker selection, no positively selected mutations are detected in our simulations. In all cases the mean cancer cell population fitness is reduced significantly if the treatment is effective. The cancer is killed off if there are no resistant sub-clones born early after treatment. The complex growth patterns of the resistant sub-clones are striking, including mixing and fast turnover (Supplementary Figure S30d, Supplementary Movies S22-S24).

Combining the findings from our general model of cancer evolution with the models of the evolutionary responses to anti-cancer therapy suggests ways to improve treatment strategies. Treatments, such as the sequential and/or cyclical use of different therapies. that lead to a faster moving phenotypic optimum (in any direction) may be more effective in killing cancer cells and help to reduce toxicity through the use of lower doses, as there is no requirement for initial maximum dosing to induce a large change in the selective optimum (Supplementary Figure S29, S31). The strategy is theoretically as effective as the classical maximum dosing in reducing mean cancer cell fitness (similar to Supplementary Movies S2-S4, Supplementary Figure S31), although it takes longer to work. Dosing strategies should, in principle, be optimized individually depending on the maximum allowed dose tolerance and the type of cancer (see Supplementary Figure S7-S9, Supplementary Movies S1-S3). In summary, although there are challenges to overcome in design and implementation, anti-cancer strategies based on moving the selective optimum appear to be highly desirable.

Discussion

We have used mathematical models and simulations to show that a changing TME of any type is highly likely to provide a barrier to carcinogenesis, especially in the early stages of growth. Faster-changing TMEs are more effective. Rapid sub-clonal shifts and "spontaneous" regression or tumour extinction may occur. There are also likely to be unobservable failed evolutionary trajectories of cancer growth and progression in human patients[1]. Our model may thus help to explain why cancer is not more common. In theory, a cancer could grow using only TME-independent driver mutations, but the

extent to which this is possible is unclear. There is evidence that even major and/or cancer-initiating driver mutations (e.g. *APC, IDH1/2, KRAS, PIK3CA,* etc) are differentially selected depending on cancer type[37], strongly suggesting a role for the TME, broadly defined, in selecting many of the common driver mutations.

Our framework does not explicitly model the TME. Rather, the TME is assumed to have a 3D space and a phenotypic optimum for cancer cells to adapt to, which can follow different changing dynamics and 3D space sizes as we have shown in this study. TMEs are highly complex in reality and challenging to model explicitly[15,26]. Therefore, this level of abstraction in our model at this stage is necessary to make advances, as this allows us to look for general patterns of cancer adaptation. Although simplistic, these phenotypic optimum change dynamics are implicated in previous studies, e.g., a directionally moving phenotypic optimum may be due to aging[38] , a variable TME may be due to dynamic immune cell infiltration[18] and a cycling TME may be due to hypoxia[24]. Overall, however, studies to determine the interaction between genotype and TME in producing a cancer phenotype are at early stages, and whilst data showing that, say, early and late cancers have very different TMEs are plentiful, data showing how the TME of an individual tumour changes are currently very limited.

There are some potential limitations to our work that could be addressed in future studies; for example, we did not model spatial heterogeneity in the same changing TME, as might occur with, for example, different immune cell infiltrations[17]. It will also be necessary to test the effects of changing TMEs in model systems, and we argue that carefully designed animal models of carcinogenesis are required for this, rather than *in vitro* TME manipulation.

Our model supports the use of therapeutic strategies that target the TME, causing the optimum to change and potentially driving the cancer cell population to extinction[1,16]. A similar approach, termed “adaptive therapy” or “metronomic chemotherapy”, has been proposed previously[39,40], where treatments have been adjusted with or without evolutionary modelling and there is clear evidence of improved patient outcome by cyclic dosing [41]. It is challenging to identify a phenotypic optimum that the cancer cells

can actually respond to, but there have been clinical trials based on this philosophy[42]. Fitness landscape-based methods could be used to measure how cancer cells adapt to treatments *in vitro* and there has been some success in measuring patient specific sub-clonal selection coefficients [43].

In conclusion, our model using phenotypic and genotypic fitness landscapes with a changing phenotypic optimum provides a single unified evolutionary and ecological framework to understand adaptive cancer evolution and treatment. Our approach is heuristic and we show that the extension of Fisher's geometric model is sufficient to produce many of the observed complex cancer evolutionary and pathology patterns. Although the phenotypic fitness landscapes are smooth, the underlying rugged genotypic landscapes of selected driver mutations due to a changing TME suggest that it is challenging to predict cancer evolution using genotypic data alone. Our focus in this study on the effect of a changing TME shows that cancers may not grow because they cannot adapt quickly enough to moving fitness optima, even if the TME changes are cyclical rather than unidirectional. In the future, our modelling framework could be used to measure heterogeneity in evolving cancers within and between patients using fitness landscapes with changing TMEs. Although most anti-cancer therapies are based on direct killing of cancer cells, use of therapy designed to cause a changing TME could lead to death through natural selection.

Methods

Fitness landscape model

In evolution, organisms can evolve by positive Darwinian selection or neutral genetic drift or a combination of both depending on how natural selection acts on the phenotypic traits and their plasticity[44]. The fitness advantage to organisms conferred by these phenotypic traits due to environmental selection can lead to adaptation[32,45,46]. In this study, we will use the metaphor of fitness landscape to understanding cancer adaptation, first introduced by Sewall Wright, which is defined by a set of genotypes, their mutational distance and fitness[45]. As our focus is to build a phenotypic and genetic

model of cancer adaptation. We first extend Fisher's geometric model of phenotypic fitness landscape to address the question of how cancer cell populations adapt to a changing tumour microenvironment[12,33,47-49] in 3D tissue space, which we assume to have a phenotypic optimum the cancer cells can adapt (note cancer cells and cancer stem cells are used interchangeably). Particularly, we extend the original Fisher's phenotypic landscape model into a general form by incorporating a moving phenotypic optimum with various changing dynamics (e.g., directionally, randomly or cyclically)[49-52]. Finally, it was suggested that the ruggedness of landscapes can determine the repeatability and predictability of adaptation[53]. We will generate and characterise the underlying Sewall Wright's genotypic landscapes of selected driver mutations from our modelling framework to explore whether such genotypic landscapes are smooth or rugged.

In Fisher's geometric framework a cancer stem cell adapting in a tumour microenvironment can be viewed as a point in an n-dimensional Euclidean phenotype space with n quantitative phenotypic traits defined by a column vector $\mathbf{z} = \left(z_1, \ldots, z_n\right)^T$. The traits involved can be any, but could for convenience be those highlighted by Hanahan and Weinberg[19]: sustaining proliferative signaling, evading growth suppressors, resisting cell death, enabling replicative immortality, angiogenesis, activating invasion and metastasis, reprogramming of energy metabolism and evading immune destruction[19]. As we assume that the TME is the primary source of selection[1,6,14,51,54-56], there is a corresponding optimum phenotype $\mathbf{z}^{opt}$, which is defined by a column vector of n values $\mathbf{z}^{opt} = \left(z_1^{opt}, \ldots, z_n^{opt}\right)^T$. The Euclidean distance, d, is defined as $d = \left\|\mathbf{z} - \mathbf{z}^{opt}\right\| = \sqrt{\sum_{k=1}^{n} (z_k - z_k^{opt})^2}$. The phenotypic fitness function for a cancer stem cell in a microenvironment is defined as[49] $w(d) = \exp\left(-ad^2\right) = \exp\left(-a\left\|\mathbf{z} - \mathbf{z}^{opt}\right\|^2\right)$. Here a is the selection intensity for all traits ($a > 0$)[49]. Therefore, the fitness of an individual cancer stem cell depends on its phenotype's Euclidean distance to the optimum. The change of phenotypic traits of a cancer stem cell due to random mutations can be

defined as an n-dimensional random number $\mathbf{r} = (r_1, \ldots, r_n)^T$. The size of a mutation (the effect of a mutation on phenotypic traits) is therefore defined as $||\mathbf{r}|| = \sqrt{r_1^2 + r_2^2 + \cdots + r_n^2}$. So, the combined phenotypic trait of a cancer stem cell $\mathbf{z}'$ with mutation $\mathbf{r}$, relative to its wild type is defined as $\mathbf{z}' = \mathbf{z} + \mathbf{r}$. We assume the phenotypic effect of a mutation with size $\mathbf{r}$ follows a multivariate normal distribution with mean $\mathbf{0}$ and $n \times n$ variance-covariance matrix $\mathbf{M}$ [48,57]. The selection coefficient of a mutation that changes the fitness of the cancer stem cell is therefore defined as

$$s \equiv \frac{w(\mathbf{z}')}{w(\mathbf{z})} - 1 = \frac{w(\mathbf{z}+\mathbf{r})}{w(\mathbf{z})} - 1, \quad (1)$$

when $s > 0$ the mutation is beneficial, it moves the cancer stem cell closer to the optimum. When the cancer stem cell is at optimum we say it has its maximum fitness $w(\mathbf{z}) = 1$, whereas when the cancer stem cell moves away from the optimum its fitness decreases ($0 \le w(\mathbf{z}) < 1$). Such mutations are deleterious and lead to negative selection coefficients with $s < 0$. When mutations do not change fitness, they are defined as neutral mutations with $s = 0$.

We can now define a general form of the fitness function as shown before[33,47,48,58].

$$w(\mathbf{z},t) = \exp\left[-\left(\mathbf{z} - \mathbf{z}^{opt}(t)\right)^T \mathbf{S}^{-1}\left(\mathbf{z} - \mathbf{z}^{opt}(t)\right)\right], (2)$$

where $\mathbf{S}$ is a real $n \times n$ positive definite and symmetrical matrix, and T denotes transposition. The matrix $\mathbf{S}$ describes the shape of the fitness landscape, namely, the selection intensity. Matrix $\mathbf{S}^{-1}$ is the inverse of $\mathbf{S}$. As introduced above, the overlapping of pathways responsible for cancer stem cell traits indicates pleiotropic effect of mutations contributing to cancer adaptive evolution[19]. If the selection intensity is the same along all n traits then we have an isotropic fitness landscape (universal pleiotropy). We set $\mathbf{S} = \sigma^2 \mathbf{I}$ ($\sigma^2 > 0$, $\mathbf{I}$ is an identity matrix). Selection may also vary

along different traits (selection is correlated), which means mutational effects contribute to fitness differently for different traits. If we set selection intensity to vary along n traits, then $\mathbf{S}$ has non-zero off-diagonal entries. We illustrate different shapes of the fitness landscape (independent and correlated selection) in Supplementary Figure S2. We can use $\bar{\sigma}^2 = \sqrt[n]{\det(\mathbf{S})}$ to measure the average width of the fitness landscape, where $\bar{\sigma}^2$ is defined as the geometric mean of the eigenvalues of $\mathbf{S}$. The selection coefficient of a mutation in equation (1) can now be defined as

$$s(\mathbf{z},\mathbf{z}',t) \equiv \frac{w(\mathbf{z}',t)}{w(\mathbf{z},t)} - 1. \qquad (3)$$

Cancer adaptation in a tumour microenvironment with a changing phenotypic optimum

In all, we consider six scenarios for how the tumour microenvironment's phenotypic optimum might change. Different initial population or individual cell properties (e.g., population size and fitness) during computer simulations are specified in the results section. We assume that the TME optimum of the first trait of the *n* traits changes[48,50].

1. Directionally changing phenotypic optimum

We assume a directionally moving optimum with $\mathbf{v}t$

$$\mathbf{z}^{opt}(t) = \mathbf{v}t, \qquad (4)$$

$$w(\mathbf{z},\mathbf{v},t) = \exp\left[-(\mathbf{z}-\mathbf{v}t)^T \mathbf{S}^{-1}(\mathbf{z}-\mathbf{v}t)\right], \qquad (5)$$

where the vector $\mathbf{v} = (v_1,\ldots,v_n)'$ is the phenotypic optimum change speed. The optimum $\mathbf{z}^{opt}(t)$ is time (generation) dependent and only the first trait optimum changes.

2. Randomly changing phenotypic optimum

Here we assume the TME optimum of the first trait, z_1^{opt}, changes randomly at each generation, t, following a Normal distribution with mean 0 and standard deviation, δ

$$\mathbf{z}^{opt}(t) = \left(z_1^{opt}, \ldots, z_n^{opt}\right), \qquad (6)$$

$$z_1^{opt} \sim N\left(0, \delta^2\right), \qquad (7)$$

$$w(\mathbf{z}, t) = \exp\left[-\left(\mathbf{z} - \mathbf{z}^{opt}(t)\right)^T \mathbf{S}^{-1}\left(\mathbf{z} - \mathbf{z}^{opt}(t)\right)\right]. \qquad (8)$$

3. Directionally changing phenotypic optimum, with a random component

We assume a directionally moving optimum with $\mathbf{v}t$ (see equation (4)) and a random component $\mathbf{e}$

$$\mathbf{z}^{opt}(t) = \mathbf{v}t + \mathbf{e}, \qquad (9)$$

$$\varepsilon_1 \sim N\left(0, \delta^2\right), (10)$$

$$w(\mathbf{z}, \mathbf{v}, \mathbf{e}, t) = \exp\left[-\left(\mathbf{z} - \mathbf{z}^{opt}(t)\right)^T \mathbf{S}^{-1}\left(\mathbf{z} - \mathbf{z}^{opt}(t)\right)\right], \quad (11)$$

where $\mathbf{v} = \left(v_1, \ldots, v_n\right)'$ is the vector of the phenotypic optimum change and it is time dependent. The random vector $\mathbf{e} = \left(\varepsilon_1, \ldots, \varepsilon_n\right)'$ has ε_1 following a random normal distribution with mean 0 and standard deviation δ.

4. Cyclically changing phenotypic optimum

In this scenario, we assume the TME optimum changes cyclically or periodically at each generation, t, following a general periodic function[50,57,59]

$$\mathbf{z}^{opt}(t) = \left(z_1^{opt}(t), \ldots, z_n^{opt}(t)\right), \quad (11)$$

$$z_1^{opt}(t) = \frac{A}{2}\left[1 + \sin\left(\frac{2\pi t}{P} - \frac{\pi}{2}\right)\right], \qquad (12)$$

$$w(\mathbf{z},t)=\exp\left[-\left(\mathbf{z}-\mathbf{z}^{opt}(t)\right)^{T}\mathbf{S}^{-1}\left(\mathbf{z}-\mathbf{z}^{opt}(t)\right)\right], \quad (13)$$

where A is the amplitude of TME optimum oscillation and P is the period (the number of generations) of the TME cycle. The equation (13) allows the TME optimum to change periodically from 0 to A and then to 0 in P generations. In all simulations of this scenario P is fixed at 360 generations.

5. Stable (i.e. constant) phenotypic optimum

We assume the TME optimum is constant with $\mathbf{z}_0^{opt}$:

$$\mathbf{z}^{opt}(t)=\mathbf{z}_0^{opt}=(z_1,\ldots,z_n), \qquad (14)$$

$$w(\mathbf{z})=\exp\left[-\left(\mathbf{z}-\mathbf{z}_0^{opt}\right)^{T}\mathbf{S}^{-1}\left(\mathbf{z}-\mathbf{z}_0^{opt}\right)\right]. \qquad (15)$$

6. Sudden change in the phenotypic optimum

We assume the TME selective optimum suddenly changes from $\mathbf{z}_0^{opt}$ to $\mathbf{z}_1^{opt}$:

$$w(\mathbf{z},t)=\begin{cases}\exp\left[-\left(\mathbf{z}-\mathbf{z}_0^{opt}\right)^{T}\mathbf{S}^{-1}\left(\mathbf{z}-\mathbf{z}_0^{opt}\right)\right], & 0\le t<\tau\\ \exp\left[-\left(\mathbf{z}-\mathbf{z}_1^{opt}\right)^{T}\mathbf{S}^{-1}\left(\mathbf{z}-\mathbf{z}_1^{opt}\right)\right], & t\ge\tau\end{cases}. \qquad (16)$$

In this scenario, the cancer cells evolve under constant stabilizing selection of the TME with optimum vector $\mathbf{z}_0^{opt}=\left(z_1^0,\ldots,z_n^0\right)'$ for τ generations. After that the TME optimum changes suddenly with a new optimum vector $\mathbf{z}_1^{opt}=\left(z_1^1,\ldots,z_n^1\right)'$ and then the cancer cells evolve under another constant stabilizing selection. For simplicity only the optimum of the first trait changes from $z_1^0=z_0^{opt}$ to $z_1^1=z_1^{opt}$ and the rest trait values are kept 0. We

set our initial TME optimum at the origin so we have vectors $\mathbf{z}_0^{opt} = \left(z_0^{opt},\ldots,0\right)'$ and

$\mathbf{z}_1^{opt} = \left(z_1^{opt},\ldots,0\right)'$ with $z_0^{opt} = 0$.

Simulation of cancer evolution in the three-dimensional space

Our intention is to identify key cancer evolutionary patterns and investigate how these are influenced by model parameters, such as the number of phenotypic traits n (the complexity of cancer cells), changing microenvironment (properties of the TME), variable selection among traits, population size, mutation rate, initial phenotype of cancer cells (distance to optimum), initial population size and chromosome instability affect cancer adaptation (tumorigenesis) in an ecological and evolutionary framework.

We simulate the cancer cell population in 3D space in one of the six environments described above (Supplementary Figure S1a). The simulation is fully individual-based, following simple growth mechanics[28,60]. In brief, the offspring of newly divided cells stochastically look for available positions in a 3D lattice space. The population evolves in a discrete and non-overlapping manner. The empty 3D tumour space represents the tumour microenvironment that may change, following the dynamics described above, and the position in the 3D space does not affect the TME or selection (except in the model extension of cell-TME interaction, see Supplementary Note 3).

Simulations are performed under particular phenotypic optimum change patterns due to either natural cause or anti-cancer therapies as described in equations (4)-(17). Here we assume cancer cells require at least one adaptive trait for survival (e.g. anti-apoptotic or metabolism related traits) as also inspired by microbial adaptive evolution[61] and mammals with very low cancer incidencies[62,63]. For simplicity we set the number of traits, $n = 2$ (the dimensionality of the fitness landscape), in each simulation unless otherwise stated. The initial population has K neoplastic cells, and grows from the centre of the specified 3D coordinates in the 3D square lattice (it has 26-cell cubic neighbours, also called a 3D Moore neighbourhood) until it reaches the defined

maximum population size or 3D tumour space, which is set at 1×10^7 and 300^3 due to computational resource limitations, respectively. The initial K cells have an adjustable phenotype $\mathbf{z}_0$. This determines the initial fitness in the fitness landscape, which has the optimum at the origin and an adjustable shape defined by $\mathbf{S}$ in equation (2) (illustrated in Supplementary Figure S2). The initial phenotype can also be calculated by equation (2) when the predefined fitness value is known. For generality we consider that the adjustable phenotype of initial K cells is determined by either classical driver mutations or phenotypic plasticity.

The cancer cells have c sets of chromosomes (ploidy) and reproduce asexually with chromosome instability (CIN). To model CIN, for simplicity we define a rate, r_c, following a Bernoulli process to vary the copy of paternal and maternal chromosome passed down to daughter cells (Supplementary Figure S1b). Each individual cancer cell is represented by L diploid loci (for computational efficiency without loss of generality $c=2$, $L=5$, unless stated otherwise) with additive effect on the n-dimensional phenotype $\mathbf{z}$.

A multifurcating tree tracks the genealogies of the alleles generated at these loci. When only one branch of an allele tree survives an adaptive step is recorded as per standard terminology[48]. The per locus mutation rate, $u=4\times10^{-5}$, is used for per genome replication [64]. Due to high mutation rate and large population size multiple mutations may be generated in each generation. So, there is clonal interference in our simulations. For this reason, we only use individual-based simulations in our study. Analytical results concerning equations (4) -(17) have previously been addressed[48,49,56,65,66]. At each generation cancer cells are removed with probability $1-w(\mathbf{z})$ as viability selection. In each simulation the population genetics parameters are recorded in files. Some simple statistics are displayed in real-time on the computer screen including time in years with 24 hours doubling time (can be adjusted if required), adaptive steps (driver mutations), generation time and population size. The reason to set the doubling time as 24 hours is to allow simulations of more generation time to gain more insights into the underlying evolutionary dynamics (e.g., one day doubling time allows roughly 37000 generations

for 100 years, however, 5 days doubling time only allows about 7400 generations). The summary statistics for population fitness and adaptive steps are sampled every 100 generations unless otherwise stated. The real-time spatial evolutionary process of the cancer development is visualized in 3D. Two-dimensional (2D) or 3D snapshots including fitness values of each cancer cell and movies are made directly from simulations.

Phylogeny reconstruction and shape measure

In our simulations, the cancer grows from single cells and each survived cell divides into two daughter cells following the branching process, so we only consider binary trees. The phylogeny or the genealogy of the evolving cancer in each simulation can be reconstructed in real-time by simply removing dead cells at each sampling point. Here we use a term called "phylodynamics" previously coined to study the shape of viral phylogenies due to the effect of evolutionary and/or ecological processes[67], which can arise due to immune selection and weak selective or non-selective forces such as space and population dynamics. Similarly, the shape of the resulting cancer phylogenies in our simulations contains useful information of the underlying evolutionary processes. In the context of our study we specifically use this term, cancer phylodynamics, to describe a similar phylodynamic framework where cancer phylogenies could be affected by both TME selection dynamics, space and cancer cell population dynamics. We use two commonly used measures of phylogeny asymmetry[68], namely the normalised Sackin's index and the number of cherries, to quantify to what extend each TME selection dynamic and 3D space (spatial constraint) affect phylogeny shapes. These measures can be very useful to infer the underlying cancer dynamics in clinical settings. Specifically, the normalized Sackin's index measures the total topological distance between the tips and the root of the tree and it is then averaged by the total number of tips, which is increasing as the tree asymmetry increases. A cherry is formed between two tips sharing a direct common ancestral node on the tree. An asymmetry tree is expected to have more cherries than a balanced tree. The two measures are complementary in measuring tree asymmetry as the former measures the overall asymmetry while the latter reveals recent asymmetry at each sampling point[69]. We used R packages

apTreeshape (https://cran.r-project.org/web/packages/apTreeshape/index.html) and treeImbalance (https://github.com/bdearlove/treeImbalance) to perform these measures.

Calculate epistasis coefficient among selected driver mutations

To further characterize the selected driver mutations and their genotypic fitness landscapes, we derive the epistasis equation between pairs of driver mutations with a moving optimum. In Fisher's fitness landscape model, based on our version of fitness function (equation (2)) the epistasis coefficient of a pair of mutations, i and j can be defined as[70]

$$e_{ij} = \log\left(\frac{w\left(\mathbf{z}_{ij},t_{ij}\right)w\left(\mathbf{z}_0,0\right)}{w\left(\mathbf{z}_i,t_i\right)w\left(\mathbf{z}_j,t_j\right)}\right), \quad (17)$$

where $w\left(\mathbf{z}_{ij},t\right)$ is the fitness of the double mutant cell while $w\left(\mathbf{z}_i,t\right)$ and $w\left(\mathbf{z}_j,t\right)$ are the fitness of the individual mutant cell. The initial ancestral cell has fitness $w_0 = w\left(\mathbf{z}_0,0\right)$ with phenotype $\mathbf{z}_0$ and the optimum is at the origin. As shown above if we define the phenotypic effect of the two mutations as $\mathbf{r}_i$ and $\mathbf{r}_j$, respectively. Then, we have the phenotype, $\mathbf{z}_i = \mathbf{z}_0 + \mathbf{r}_i$, for the mutant cell carrying the mutation i and phenotype, $\mathbf{z}_j = \mathbf{z}_0 + \mathbf{r}_j$, for the mutant cell carrying the mutation j. The phenotype of the double mutant is $\mathbf{z}_{ij} = \mathbf{z}_0 + \mathbf{r}_i + \mathbf{r}_j$. Similarly, the TME optima are $\mathbf{z}_i^{opt}(t)$ and $\mathbf{z}_j^{opt}(t)$ for mutant cells carrying mutations i and j, respectively. The optimum for the double mutant can be defined as $\mathbf{z}_{ij}^{opt}(t_{ij}) = \mathbf{z}_i^{opt}(t_i) + \mathbf{z}_j^{opt}(t_j)$. The above epistasis coefficient in a changing TME can be further given as

$$e_{ij} = -2(\mathbf{r}_i - \mathbf{z}_i^{opt}(t_i))^T \mathbf{S}^{-1}(\mathbf{r}_j - \mathbf{z}_j^{opt}(t_j)). \qquad (18)$$

Note that, here the epistasis is also affected by the changing TME optimum and the epistasis coefficients between pairs of mutations can be directly calculated from the simulations.

Properties of a genotypic landscape of selected driver mutations

The ruggedness of cancer genotypic landscapes may determine the predictability and repeatability of cancer adaptation and therefore of paramount importance for managing cancer[53]. When describing a genotypic landscape four to five genotypes are typically used. This leads to 2^4 or 2^5 all possible combinations of these genotypes to form a genotypic landscape. The epistasis coefficient between two mutations can be calculated when we know the fitness effect of the mutants as shown above. For simplicity, in our study we use four selected driver mutations to summarise the genotypic landscapes generated by the extended Fisher's fitness landscape model with a changing phenotypic optimum. We further summarize these genotypic landscapes using two commonly used summary statistics[53], namely, the fraction of sign epistasis and roughness to slope ratio[71,72]. The former defines a situation where the fitness effect of driver mutations depends on their background driver mutations. The later quantifies how well a landscape can be described by a linear model where driver mutations can additively determine their fitness. There are two types of sign epistasis: simple and reciprocal (complex) sign epistasis. In simple sign epistasis only one of the driver mutations is deleterious with the other driver mutation, while in complex sign epistasis both driver mutations are deleterious with the other driver mutation as its background driver mutation, which could only happen in a cycling TME in our study.

Author contributions

XJ and IPMT conceived the study. XJ developed the model and implemented the computational framework and performed the simulations. XJ and IPMT analysed the simulation results. XJ and IPMT wrote the manuscript.

Acknowledgements

XJ is supported by an ERC advanced grant (EVOCAN-340560) awarded to IPMT. We thank John Welch and Sebastian Matuszewski for helpful discussion of the Fisher's geometric model, and Sebastian Matuszewski and Andrea Sottoriva for providing their publication materials. We are grateful to Shazia Irshad and members of the Tomlinson laboratory for cancer biology discussions. We also thank Martijn Koppens, Roland Arnold and Yun Feng for helpful comments of the manuscript. We thank Robert Esnouf and Jonathan Diprose from Oxford Wellcome Trust Centre for Human Genetics Research Computing Core for computing assistance.

References

1 Bissell, M. J. & Hines, W. C. Why don't we get more cancer? A proposed role of the microenvironment in restraining cancer progression. *Nat Med* **17**, 320-329, doi:10.1038/nm.2328 (2011).

2 Fridman, W. H., Zitvogel, L., Sautes-Fridman, C. & Kroemer, G. The immune contexture in cancer prognosis and treatment. *Nat Rev Clin Oncol*, doi:10.1038/nrclinonc.2017.101 (2017).

3 Vermeulen, L. *et al.* Defining stem cell dynamics in models of intestinal tumor initiation. *Science* **342**, 995-998, doi:10.1126/science.1243148 (2013).

4 Paget, S. The Distribution of Secondary Growths in Cancer of the Breast. *The Lancet* **133**, 571-573, doi:10.1016/s0140-6736(00)49915-0 (1889).

5 Nowell, P. C. The clonal evolution of tumor cell populations. *Science* **194**, 23-28 (1976).

6 Tomlinson, I. Mutations, evolutionary theory and cancer. *Trends Ecol Evol* **8**, 107-110, doi:10.1016/0169-5347(93)90062-T (1993).

7 Liotta, L. A. & Kohn, E. C. The microenvironment of the tumour-host interface. *Nature* **411**, 375-379, doi:10.1038/35077241 (2001).

8 Merlo, L. M., Pepper, J. W., Reid, B. J. & Maley, C. C. Cancer as an evolutionary and ecological process. *Nat Rev Cancer* **6**, 924-935, doi:10.1038/nrc2013 (2006).

9 Korolev, K. S., Xavier, J. B. & Gore, J. Turning ecology and evolution against cancer. *Nat Rev Cancer* **14**, 371-380, doi:10.1038/nrc3712 (2014).

10 Crespi, B. & Summers, K. Evolutionary biology of cancer. *Trends Ecol Evol* **20**, 545-552, doi:10.1016/j.tree.2005.07.007 (2005).

11 Vogelstein, B. & Kinzler, K. W. The multistep nature of cancer. *Trends Genet* **9**, 138-141 (1993).

12 Orr, H. A. The genetic theory of adaptation: a brief history. *Nat Rev Genet* **6**, 119-127, doi:10.1038/nrg1523 (2005).

13 Gatenby, R. A. & Gillies, R. J. A microenvironmental model of carcinogenesis. *Nat Rev Cancer* **8**, 56-61, doi:10.1038/nrc2255 (2008).

14 Junttila, M. R. & de Sauvage, F. J. Influence of tumour micro-environment heterogeneity on therapeutic response. *Nature* **501**, 346-354, doi:10.1038/nature12626 (2013).

15 Quail, D. F. & Joyce, J. A. Microenvironmental regulation of tumor progression and metastasis. *Nat Med* **19**, 1423-1437, doi:10.1038/nm.3394 (2013).

16 Tauriello, D. V. F. & Batlle, E. Targeting the Microenvironment in Advanced Colorectal Cancer. *Trends in Cancer*, doi:10.1016/j.trecan.2016.08.001 (2016).

17 Jimenez-Sanchez, A. *et al.* Heterogeneous Tumor-Immune Microenvironments among Differentially Growing Metastases in an Ovarian Cancer Patient. *Cell* **170**, 927-938 e920, doi:10.1016/j.cell.2017.07.025 (2017).

18 Zhang, A. W. *et al.* Interfaces of Malignant and Immunologic Clonal Dynamics in Ovarian Cancer. *Cell* **173**, 1755-1769 e1722, doi:10.1016/j.cell.2018.03.073 (2018).

19 Hanahan, D. & Weinberg, R. A. Hallmarks of cancer: the next generation. *Cell* **144**, 646-674, doi:10.1016/j.cell.2011.02.013 (2011).

20 Lan, C. *et al.* Quantitative histology analysis of the ovarian tumour microenvironment. *Sci Rep* **5**, 16317, doi:10.1038/srep16317 (2015).
21 Zhang, L. *et al.* Microenvironment-induced PTEN loss by exosomal microRNA primes brain metastasis outgrowth. *Nature* **527**, 100-104, doi:10.1038/nature15376 (2015).
22 Hawkins, E. D. *et al.* T-cell acute leukaemia exhibits dynamic interactions with bone marrow microenvironments. *Nature* **538**, 518-522, doi:10.1038/nature19801 (2016).
23 Liu, Y. & Cao, X. Characteristics and Significance of the Pre-metastatic Niche. *Cancer Cell* **30**, 668-681, doi:10.1016/j.ccell.2016.09.011 (2016).
24 Dewhirst, M. W., Cao, Y. & Moeller, B. Cycling hypoxia and free radicals regulate angiogenesis and radiotherapy response. *Nat Rev Cancer* **8**, 425-437, doi:10.1038/nrc2397 (2008).
25 Rankin, E. B. & Giaccia, A. J. Hypoxic control of metastasis. *Science* **352**, 175-180, doi:10.1126/science.aaf4405 (2016).
26 Altrock, P. M., Liu, L. L. & Michor, F. The mathematics of cancer: integrating quantitative models. *Nat Rev Cancer* **15**, 730-745, doi:10.1038/nrc4029 (2015).
27 Tomlinson, I. P. & Bodmer, W. F. Modelling the consequences of interactions between tumour cells. *Br J Cancer* **75**, 157-160 (1997).
28 Waclaw, B. *et al.* A spatial model predicts that dispersal and cell turnover limit intratumour heterogeneity. *Nature* **525**, 261-264, doi:10.1038/nature14971 (2015).
29 Sottoriva, A. *et al.* A Big Bang model of human colorectal tumor growth. *Nat Genet* **47**, 209-216, doi:10.1038/ng.3214 (2015).
30 Anderson, A. R., Weaver, A. M., Cummings, P. T. & Quaranta, V. Tumor morphology and phenotypic evolution driven by selective pressure from the microenvironment. *Cell* **127**, 905-915, doi:10.1016/j.cell.2006.09.042 (2006).
31 Lloyd, M. C. *et al.* Darwinian Dynamics of Intratumoral Heterogeneity: Not Solely Random Mutations but Also Variable Environmental Selection Forces. *Cancer Res* **76**, 3136-3144, doi:10.1158/0008-5472.CAN-15-2962 (2016).
32 Fisher, R. A. *The genetical theory of natural selection*. (The Clarendon press, 1930).
33 Waxman, D. & Welch, J. J. Fisher's microscope and Haldane's ellipse. *Am Nat* **166**, 447-457, doi:10.1086/444404 (2005).
34 Davis, H. *et al.* Aberrant epithelial GREM1 expression initiates colonic tumorigenesis from cells outside the stem cell niche. *Nat Med* **21**, 62-70, doi:10.1038/nm.3750 (2015).
35 Castro-Giner, F., Ratcliffe, P. & Tomlinson, I. The mini-driver model of polygenic cancer evolution. *Nat Rev Cancer* **15**, 680-685, doi:10.1038/nrc3999 (2015).
36 Barnett, G. C. *et al.* Normal tissue reactions to radiotherapy: towards tailoring treatment dose by genotype. *Nat Rev Cancer* **9**, 134-142, doi:10.1038/nrc2587 (2009).
37 Temko, D., Tomlinson, I. P. M., Severini, S., Schuster-Bockler, B. & Graham, T. A. The effects of mutational processes and selection on driver mutations across cancer types. *Nat Commun* **9**, 1857, doi:10.1038/s41467-018-04208-6 (2018).

38 de Magalhaes, J. P. How ageing processes influence cancer. *Nat Rev Cancer* **13**, 357-365, doi:10.1038/nrc3497 (2013).
39 Gatenby, R. A., Silva, A. S., Gillies, R. J. & Frieden, B. R. Adaptive therapy. *Cancer Res* **69**, 4894-4903, doi:10.1158/0008-5472.CAN-08-3658 (2009).
40 Kerbel, R. S. & Kamen, B. A. The anti-angiogenic basis of metronomic chemotherapy. *Nat Rev Cancer* **4**, 423-436, doi:10.1038/nrc1369 (2004).
41 Zhang, J., Cunningham, J. J., Brown, J. S. & Gatenby, R. A. Integrating evolutionary dynamics into treatment of metastatic castrate-resistant prostate cancer. *Nat Commun* **8**, 1816, doi:10.1038/s41467-017-01968-5 (2017).
42 Joyce, J. A. Therapeutic targeting of the tumor microenvironment. *Cancer Cell* **7**, 513-520, doi:10.1016/j.ccr.2005.05.024 (2005).
43 Williams, M. J. *et al.* Quantification of subclonal selection in cancer from bulk sequencing data. *Nat Genet* **50**, 895-903, doi:10.1038/s41588-018-0128-6 (2018).
44 Hughes, A. L. Evolution of adaptive phenotypic traits without positive Darwinian selection. *Heredity* **108**, 347-353, doi:10.1038/hdy.2011.97 (2012).
45 Wright, S. The roles of mutation, inbreeding, crossbreeding, and selection in evolution. *Proceedings of the Sixth International Congress of Genetics* **1**, 356-366 (1932).
46 Haldane, J. B. S. *The causes of evolution*. (Longmans, Green and co., 1932).
47 Martin, G. & Lenormand, T. A general multivariate extension of Fisher's geometrical model and the distribution of mutation fitness effects across species. *Evolution* **60**, 893-907 (2006).
48 Matuszewski, S., Hermisson, J. & Kopp, M. Fisher's geometric model with a moving optimum. *Evolution* **68**, 2571-2588, doi:10.1111/evo.12465 (2014).
49 Tenaillon, O. The Utility of Fisher's Geometric Model in Evolutionary Genetics. *Annu Rev Ecol Evol Syst* **45**, 179-201, doi:10.1146/annurev-ecolsys-120213-091846 (2014).
50 Fraisse, C., Gunnarsson, P. A., Roze, D., Bierne, N. & Welch, J. J. The genetics of speciation: Insights from Fisher's geometric model. *Evolution* **70**, 1450-1464, doi:10.1111/evo.12968 (2016).
51 Lourenco, J. M., Glemin, S. & Galtier, N. The rate of molecular adaptation in a changing environment. *Mol Biol Evol* **30**, 1292-1301, doi:10.1093/molbev/mst026 (2013).
52 Razeto-Barry, P., Diaz, J. & Vasquez, R. A. The nearly neutral and selection theories of molecular evolution under the fisher geometrical framework: substitution rate, population size, and complexity. *Genetics* **191**, 523-534, doi:10.1534/genetics.112.138628 (2012).
53 Blanquart, F., Achaz, G., Bataillon, T. & Tenaillon, O. Properties of selected mutations and genotypic landscapes under Fisher's geometric model. *Evolution* **68**, 3537-3554, doi:10.1111/evo.12545 (2014).
54 Tomlinson, I. & Bodmer, W. Selection, the mutation rate and cancer: ensuring that the tail does not wag the dog. *Nat Med* **5**, 11-12, doi:10.1038/4687 (1999).
55 Waxman, D. & Peck, J. R. Sex and adaptation in a changing environment. *Genetics* **153**, 1041-1053 (1999).
56 Kopp, M. & Hermisson, J. The genetic basis of phenotypic adaptation II: the distribution of adaptive substitutions in the moving optimum model. *Genetics* **183**, 1453-1476, doi:10.1534/genetics.109.106195 (2009).

57 Zhang, X. S. Fisher's geometrical model of fitness landscape and variance in fitness within a changing environment. *Evolution* **66**, 2350-2368, doi:10.1111/j.1558-5646.2012.01610.x (2012).
58 Waxman, D. Fisher's geometrical model of evolutionary adaptation--beyond spherical geometry. *J Theor Biol* **241**, 887-895, doi:10.1016/j.jtbi.2006.01.024 (2006).
59 Charlesworth, B. Directional selection and the evolution of sex and recombination. *Genet Res* **61**, 205-224 (1993).
60 Sottoriva, A., Spiteri, I., Shibata, D., Curtis, C. & Tavare, S. Single-molecule genomic data delineate patient-specific tumor profiles and cancer stem cell organization. *Cancer Res* **73**, 41-49, doi:10.1158/0008-5472.CAN-12-2273 (2013).
61 Elena, S. F., Cooper, V. S. & Lenski, R. E. Punctuated evolution caused by selection of rare beneficial mutations. *Science* **272**, 1802-1804 (1996).
62 Seluanov, A. *et al.* Hypersensitivity to contact inhibition provides a clue to cancer resistance of naked mole-rat. *Proc Natl Acad Sci U S A* **106**, 19352-19357, doi:10.1073/pnas.0905252106 (2009).
63 Sulak, M. *et al.* TP53 copy number expansion is associated with the evolution of increased body size and an enhanced DNA damage response in elephants. *Elife* **5**, doi:10.7554/eLife.11994 (2016).
64 Bozic, I. *et al.* Accumulation of driver and passenger mutations during tumor progression. *Proc Natl Acad Sci U S A* **107**, 18545-18550, doi:10.1073/pnas.1010978107 (2010).
65 Kopp, M. & Hermisson, J. The genetic basis of phenotypic adaptation I: fixation of beneficial mutations in the moving optimum model. *Genetics* **182**, 233-249, doi:10.1534/genetics.108.099820 (2009).
66 Martin, G. & Lenormand, T. The fitness effect of mutations across environments: Fisher's geometrical model with multiple optima. *Evolution* **69**, 1433-1447, doi:10.1111/evo.12671 (2015).
67 Grenfell, B. T. *et al.* Unifying the epidemiological and evolutionary dynamics of pathogens. *Science* **303**, 327-332, doi:10.1126/science.1090727 (2004).
68 Blum, M. G. & Francois, O. On statistical tests of phylogenetic tree imbalance: the Sackin and other indices revisited. *Math Biosci* **195**, 141-153, doi:10.1016/j.mbs.2005.03.003 (2005).
69 Dearlove, B. L. & Frost, S. D. Measuring Asymmetry in Time-Stamped Phylogenies. *PLoS Comput Biol* **11**, e1004312, doi:10.1371/journal.pcbi.1004312 (2015).
70 Martin, G., Elena, S. F. & Lenormand, T. Distributions of epistasis in microbes fit predictions from a fitness landscape model. *Nat Genet* **39**, 555-560, doi:10.1038/ng1998 (2007).
71 Carneiro, M. & Hartl, D. L. Colloquium papers: Adaptive landscapes and protein evolution. *Proc Natl Acad Sci U S A* **107 Suppl 1**, 1747-1751, doi:10.1073/pnas.0906192106 (2010).
72 Szendro, I. G., Schenk, M. F., Franke, J., Krug, J. & de Visser, J. A. G. M. Quantitative analyses of empirical fitness landscapes. *Journal of Statistical Mechanics: Theory and Experiment* **2013**, P01005, doi:10.1088/1742-5468/2013/01/p01005 (2013).

Figure Legends

Figure 1. 3D simulation snapshots of cancer adaptive evolution under various directionally changing TME selective optima.

Illustrative 3D snapshots of the evolving cancer cell population are taken sequentially, under different phenotypic optimum change rates, v_1. **a-c**, $v_1 = 0.05$. **d-f**, $v_1 = 5 \times 10^{-3}$. **g-i**, $v_1 = 5 \times 10^{-4}$. **j-l**, $v_1 = 5 \times 10^{-5}$. To illustrate sub-clonal heterogeneity of fitness through time and 3D space, cancer cells are coloured according to their fitness cut-off values using quartiles, which results in four groups of cancer cells colored with four different colors: red (the highest 25%), cyan (between the highest 25% and 50%), grey (between the lowest 50% and 25%) and green (the lowest 25%), respectively. To show 3D mixing of sub-clones with different fitness, we applied lower opacity to cyan, grey and green colors representing the lowest 75% cancer cell populations in fitness. Note that, because of immediate population extinction, data are not shown for simulations with phenotypic optimum change rate at $v_1 = 0.5$. The width of the fitness landscape (i.e. selection intensity) is set to $\sigma^2 = 10$ (equation (2) and Supplementary Figure S2).

Figure 2. Representative cancer evolution trajectories with different rates of directionally changing TME selective optima.

a, the mean population fitness of the evolving cancer cells is sampled at various phenotypic optimum change rates. The dashed line represents mean fitness 0.5. When mean population fitness reaches this value it is more likely to be extinct. The line represents a simple linear regression fit. **b**, the mean selection coefficients are sampled at various phenotypic optimum change rates. The line represents a smooth curve. **c**, the mean selection coefficients are plotted against the phenotypic optimum change rates. **d**, the mean population fitness is plotted against the number of traits of cancer cells. **e**, the mean selection coefficients are plotted against the number of traits of cancer cells. The TME rates used are $v_1 = 0.5$, $v_1 = 0.05$, $v_1 = 5 \times 10^{-3}$, $v_1 = 5 \times 10^{-4}$ and $v_1 = 5 \times 10^{-5}$. Note that, because of immediate population extinction data are not shown for simulations

with phenotypic optimum change rate at $v_1 = 0.5$. Error bars are the standard error of the mean (s.e.m.), and each point represents 100 independent simulations.

Figure 3. Cancer adaptive evolution under multiple different initial conditions. Simulations are performed with different initial conditions regarding population size, fitness and TME optimum changing rates. Three conditions for initial population size are used, $N = 10$ (coloured blue), $N = 10^4$ (coloured red) and $N = 10^7$ (coloured green), respectively. Three conditions for initial fitness are also used, $w = 0.1$ (**a-d**), $w = 0.5$ (**e-h**) and $w = 0.9$ (**i-l**). Populations also evolve under four different phenotypic optimum change rates: $v_1 = 5 \times 10^{-5}$ (**a, e** and **i**), $v_1 = 5 \times 10^{-4}$ (**b**, **f** and **j**), $v_1 = 5 \times 10^{-3}$ (**c**, **g** and **k**) and $v_1 = 0.05$ (**d**, **h** and **l**), respectively. Error bars are s.e.m. and each point represents 100 independent simulations. Note that in **e-l** all color lines are present, but they are too close to each other to be seen clearly.

Figure 4*. Cancer phylogenies under directionally changing TME selection dynamics.* These results demonstrate that it is possible to use cancer phylogenies to understand the underlying TME selection dynamics due to either cancer treatments or somatic evolution. Example phylogenies are shown for simulated cancers under three different TME selective dynamics. **a-d**, four illustrative phylogenies are shown for a directionally changing TME with four different speeds: $v_1 = 0$ (static TME, **a**), $v_1 = 5 \times 10^{-5}$ (**b**), $v_1 = 5 \times 10^{-4}$ (**c**) and $v_1 = 5 \times 10^{-3}$ (**d**). All cancers were longitudinally sampled for every 100 generations for a fixed period of time of 10000 generations except (**d**), where the cancer went extinct at approximately 2300 generations. The maximum population size is set at $N = 10^5$. The scale bar represents the number of cell divisions.

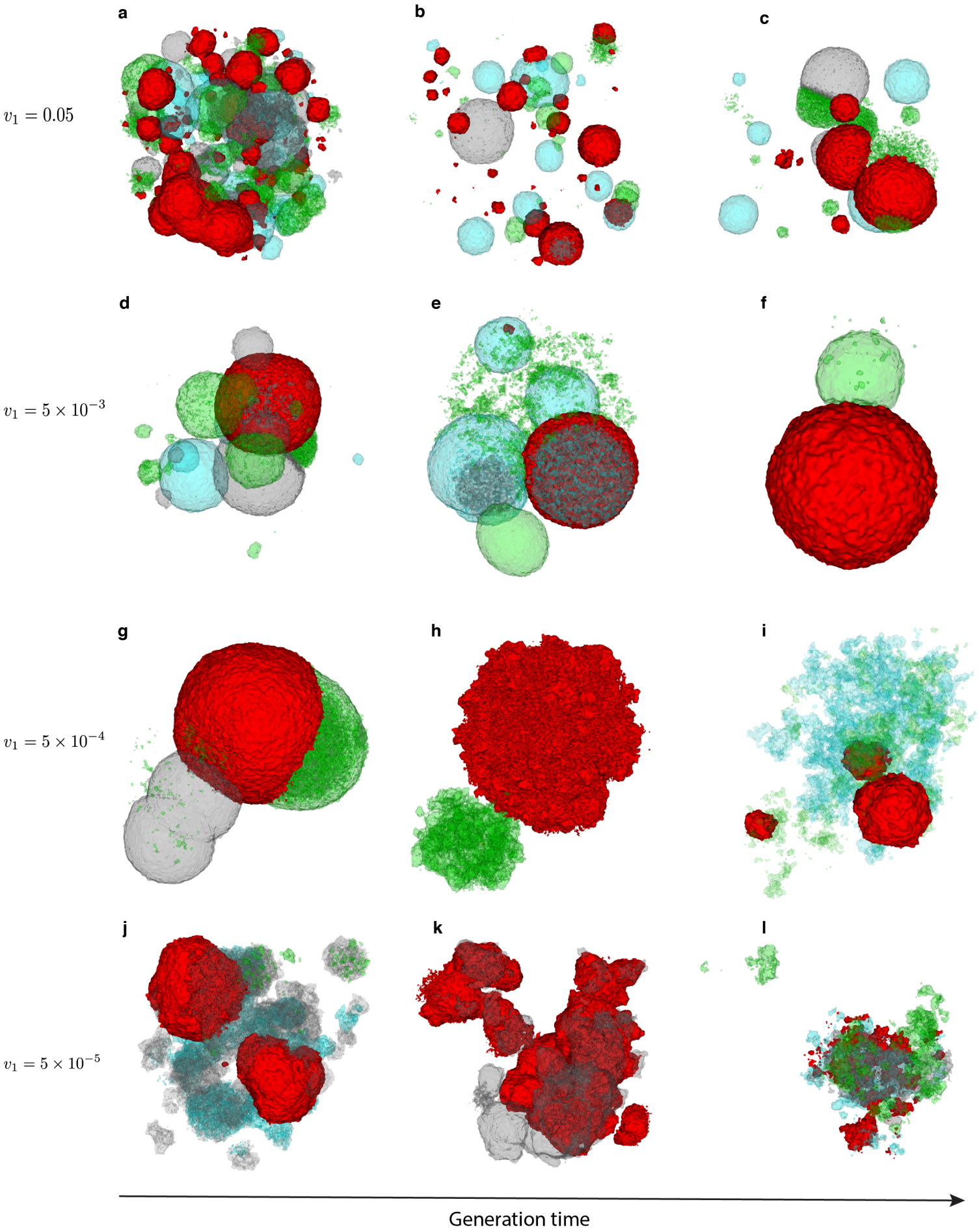
a
b
c
$v_1 = 0.05$
d
e
f
$v_1 = 5 \times 10^{-3}$
g
h
i
$v_1 = 5 \times 10^{-4}$
j
k
l
$v_1 = 5 \times 10^{-5}$
Generation time

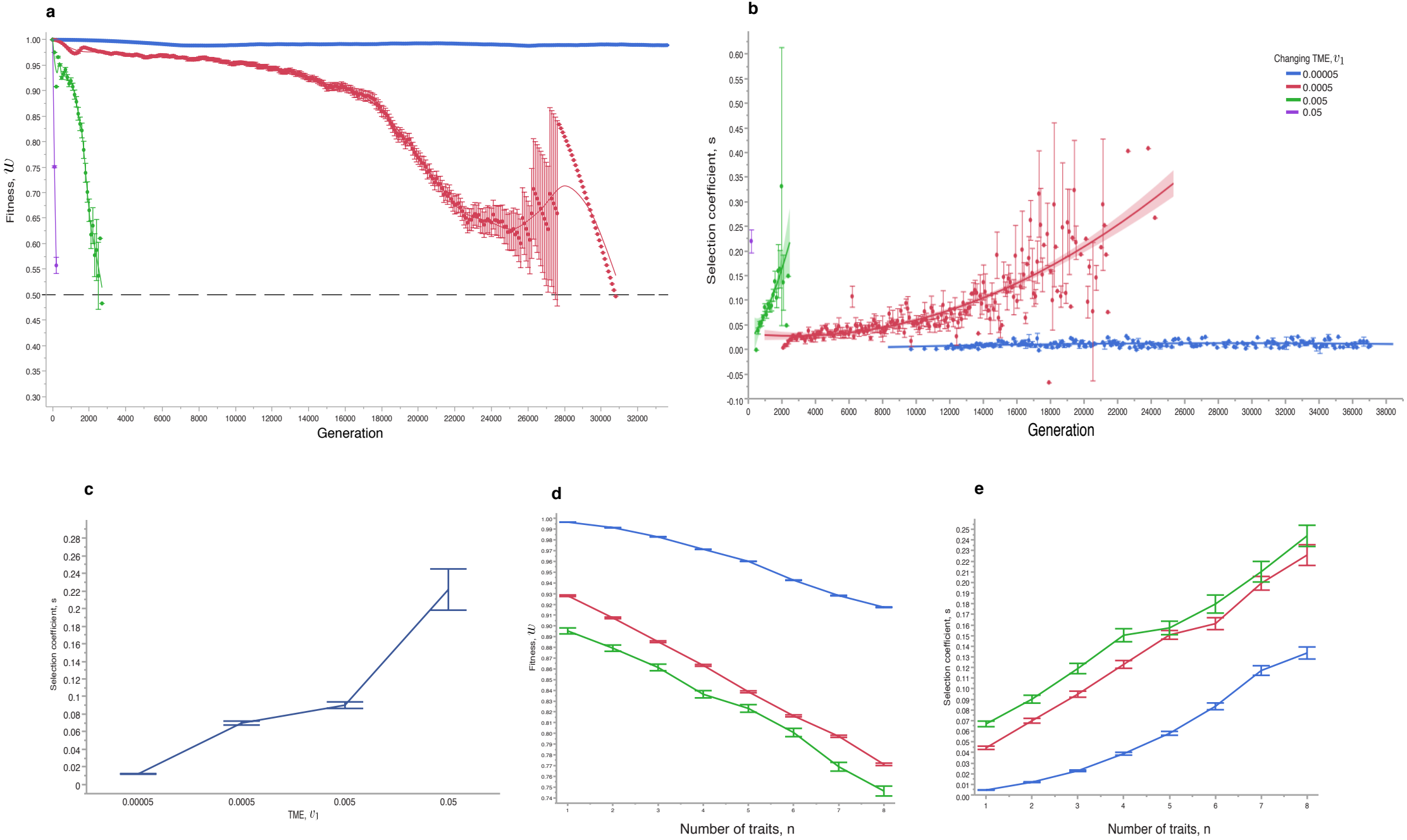
a
Fitness, w
Generation
b
Selection coefficient, s
Generation
Changing TME, v_1
0.00005
0.0005
0.005
0.05
c
Selection coefficient, s
TME, v_1
0.00005
0.0005
0.005
0.05
d
Fitness, w
Number of traits, n
e
Selection coefficient, s
Number of traits, n

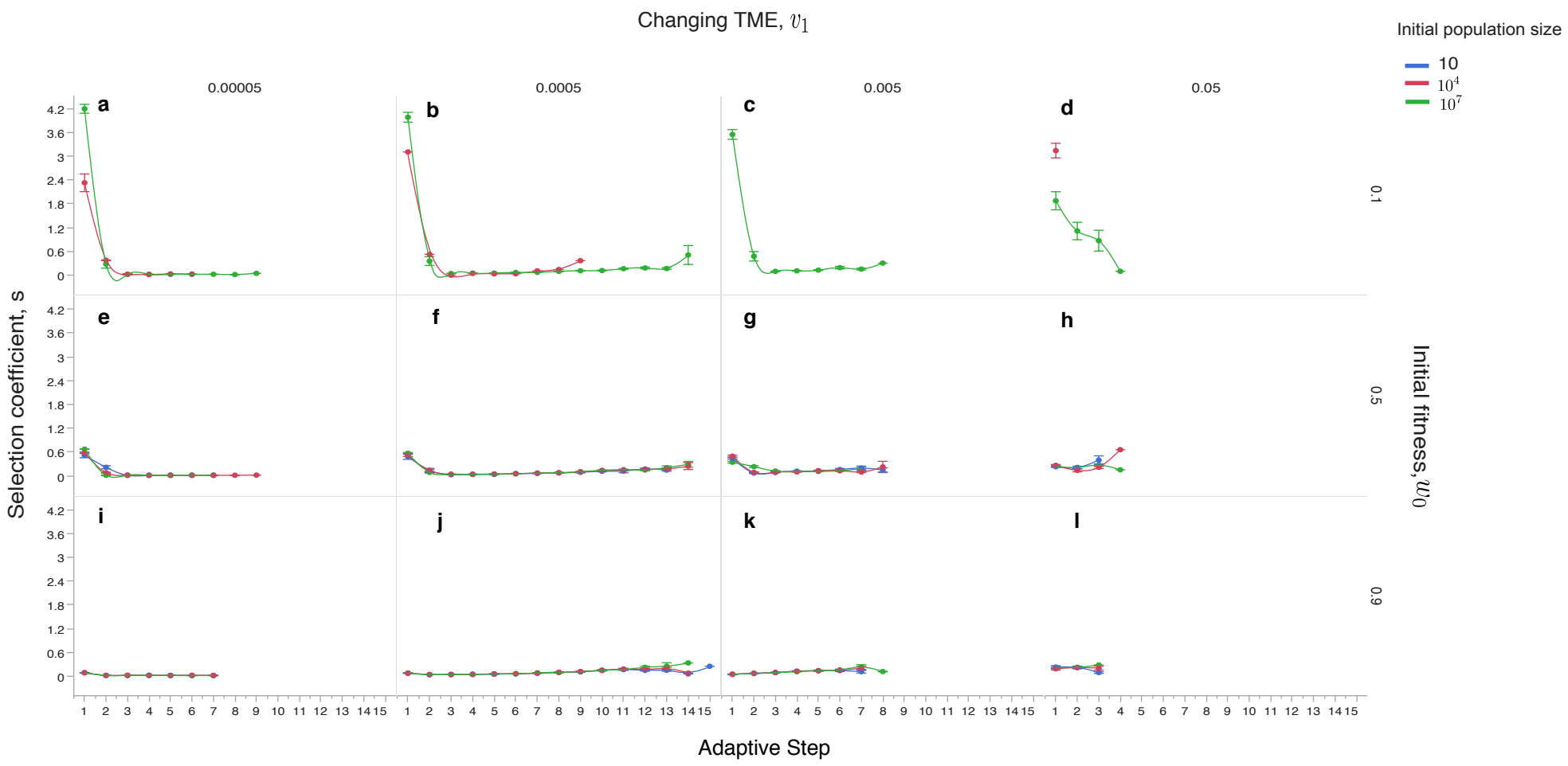
Changing TME, v_1
Initial population size
10
10^4
10^7
0.00005
0.0005
0.005
0.05
0.1
0.5
0.9
Initial fitness, u_0
Selection coefficient, s
Adaptive Step
a
b
c
d
e
f
g
h
i
j
k
l

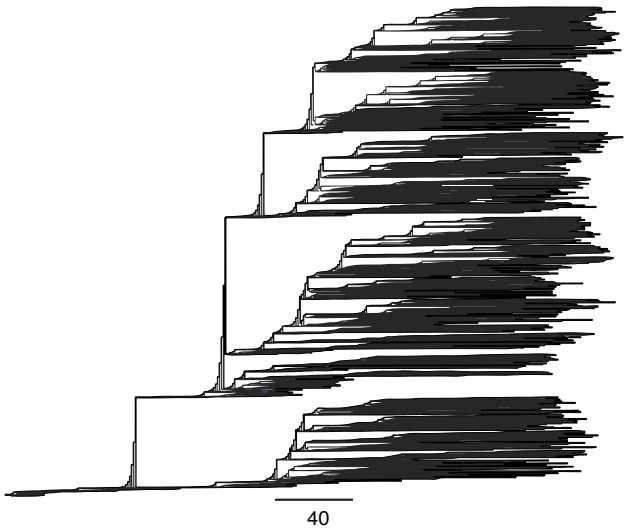

a

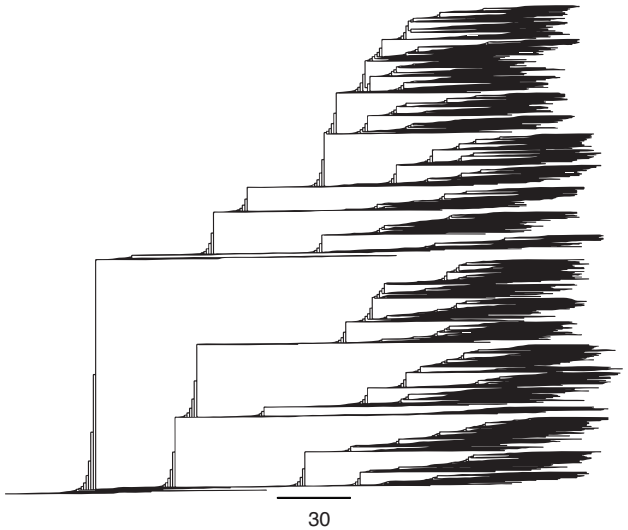

b

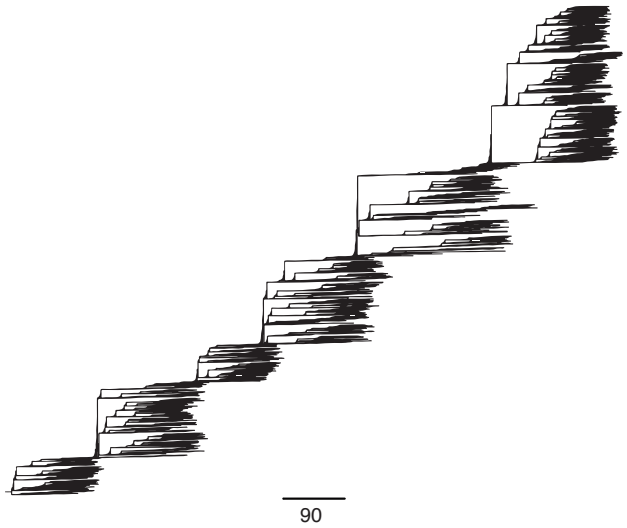

c

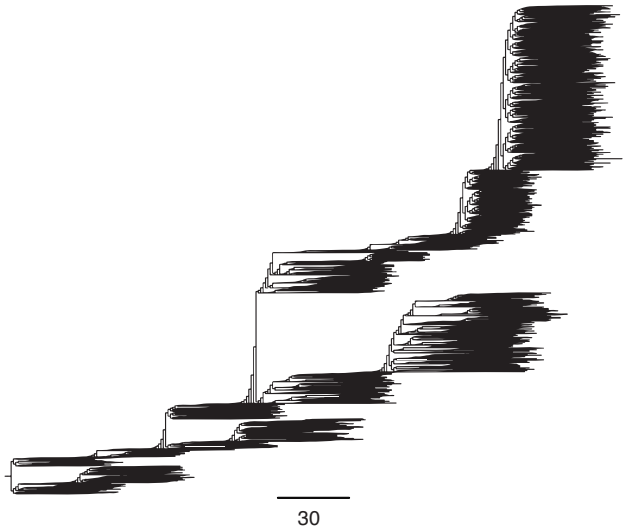

d